High-Efficiency Nanostructured Silicon Solar Cells on a Large Scale Realized Through the Suppression of Recombination Channels

*Sihua Zhong, Zengguang Huang, Xingxing Lin, Yang Zeng, Yechi Ma, and Wenzhong Shen**

Nanostructured silicon solar cells show great potential for new-generation photovoltaics due to their ability to approach ideal light-trapping. However, the nanofeatured morphology that brings about the optical benefits also introduces new recombination channels, and severe deterioration in the electrical performance even outweighs the gain in optics in most attempts. This Research News article aims to review the recent progress in the suppression of carrier recombination in silicon nanostructures, with the emphasis on the optimization of surface morphology and controllable nanostructure height and emitter doping concentration, as well as application of dielectric passivation coatings, providing design rules to realize high-efficiency nanostructured silicon solar cells on a large scale.

1. Introduction

Silicon nanostructures are believed to be prominent platforms for the next generation of high-efficiency photovoltaic devices due to their ideal antireflection characteristics.[1–5] Near-zero reflection over a broad wavelength range can be achieved,[6–8] resulting in the so-called "black silicon". These silicon nanostructures also have the ability to effectively suppress the surface reflection over a wide range of incident angles, which is extremely beneficial for solar-power applications.[9–14] Such superior antireflection features are primarily attributed to the subwavelength dimensions of the silicon nanostructures, which form a gradient of refractive index and suppress Fresnel reflection.[11,13] Therefore, significant efforts have been devoted to implementing silicon nanostructures into various solar cells, including diffused *p–n* junction cells,[15–20] photo-electrochemical cells,[21,22] solid-state hybrid heterojunction cells,[23] and thin film cells.[24]

The conversion efficiencies (η) of nanostructured silicon solar cells are still far from satisfactory, especially when compared to the records of the conventional counterparts. The main obstacle for achieving high η is that the degradation of the electrical properties caused by the accelerated recombination of the photogenerated carriers often outweighs the benefit of the improved optical absorption. The severe carrier recombination comes from the enhanced surface and emitter bulk recombination in the silicon nanostructures, which are associated with the increased surface area and the enlarged volume of the heavily doped emitter, respectively. Thus, it has been widely accepted that the suppression of these recombination channels is of paramount importance to the performance enhancement of the nanostructured silicon solar cells. In the following, we review the recent progress in the suppression of carrier recombination in silicon nanostructures, including the optimization of surface morphology (such as multiscale surface texture,[25,26] optimizing nanostructure density,[27] novel silicon nanostructures with low surface area enhancement,[28,29] control over the nanostructure height,[16,18,30] application of various dielectric passivation coatings[16,31–34] and reducing emitter doping concentration.[35] **Figure 1**a shows the multiscale surface texture containing micrometer scale pyramid-like structures and silicon nanostructures, together with countermeasures to suppress the recombination channels. This Research News article shows that, under present industrial manufacture processes, the successful suppression of carrier recombination and the realization of high-performance nanostructured silicon solar cells with a large size is acheived, which opens potential prospects for the mass production of high-efficiency nanostructured silicon solar cells.

2. Control of Surface Recombination by Optimizing the Surface Morphology

Surface recombination in nanostructures is directly related to surface morphology. Considerable interest has been focused on the optimization of surface morphology (mainly including multiscale texture, silicon nanostructure density, and novel silicon nanostructures with low surface area enhancement) to reduce the surface area and hence surface recombination. A multiscale surface texture, which is realized by incorporating

S. H. Zhong, Z. G. Huang, X. X. Lin, Y. Zeng, Y. C. Ma, Prof. W. Z. Shen
Institute of Solar Energy, and Key Laboratory of Artificial Structures and Quantum Control (Ministry of Education)
Department of Physics and Astronomy
Shanghai Jiao Tong University
800 Dong Chuan Road, Shanghai 200240, PR China
E-mail: wzshen@sjtu.edu.cn

DOI: 10.1002/adma.201401553

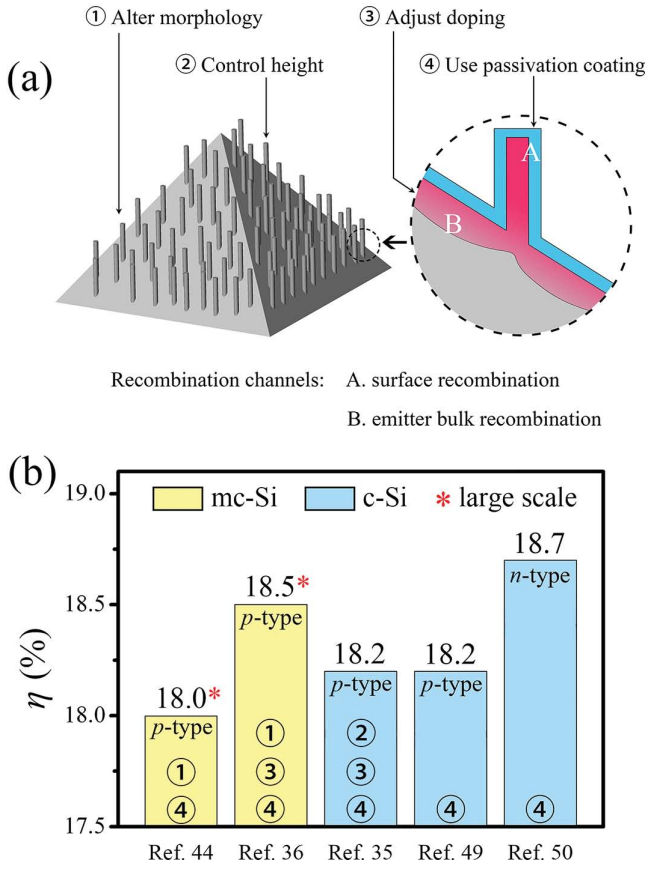

Figure 1. a) Schematic of the multiscale surface texture containing micrometer scale pyramid-like structures and silicon nanostructures. The four countermeasures to suppress the two recombination channels are labeled. b) A summary of the latest high-efficiency nanostructured silicon solar cells and their main recombination suppression techniques. Here c-Si and mc-Si denote the crystalline and multicrystalline silicon, respectively.

silicon nanostructures into the crystalline silicon (c-Si) micrometer-scale pyramid texture (see **Figure 2**a), has been proposed to reduce the surface recombination.[25] It has been found that a nanostructure height of only 100 nm is sufficient for obtaining a solar-spectrum-weighted average reflectance below 2% based on this multiscale texture technique, while a height of 250 nm is needed to obtain such low reflectance for planar nanostructured samples. Obviously, multiscale-textured silicon can retain an excellent surface antireflection property even when the nanostructures are much shorter than that on the planar surface due to the combined advantages of geometric optics from micrometer-scale pyramid and a graded effective refractive index from nanostructures. This indicates that the use of multiscale texture allows thinning the nanostructured layers to reduce surface recombination while maintaining ultra-low reflectance. As a result, the blue spectral response is substantially improved from 57% to 71% at the wavelength of 450 nm, and an η of 17.1% has been realized for nanostructured silicon solar cells.[25] Lee et al.[26] have also adopted this multiscale texture technique and studied the influence of the nanostructure height on the cell performance, demonstrating that a tradeoff between surface reflection and carrier recombination is the key to obtaining an optimal η. The idea of multiscale texture has also been widely applied in enhancing the η of nanostructured multicrystalline silicon (mc-Si) solar cells, where the micrometer-scale pyramids are replaced by micrometer-scale bowl-like structures (see Figure 2b). Based on the multiscale surface texture, Liu et al.[36] have recently reported an 18.49%-efficient large-scale nanostructured mc-Si solar cell. It is worth mentioning that the multiscale texture is also extremely effective in restraining the surface carrier recombination and enhance the η of Si/polymer hybrid solar cells.[23]

Optimization of the silicon nanostructure density is another important aspect in enhancing the performance of nanostructured silicon solar cells. It is interesting to note that the surface reflectance and the minority carrier lifetime exhibit the same variation trend versus the silicon nanostructure density;[37] namely, as the silicon nanostructure density increases to a certain value (such as 70%), both the surface reflectance and the minority carrier lifetime decrease due to the decreased effective refractive indices and increased effective surface area, respectively. When further increasing the silicon nanostructure density beyond this value, both the surface reflectance and the minority carrier lifetime increase as the results of increased effective refractive indices and reduced effective surface area, respectively. Obviously, the density of the silicon nanostructures can significantly affect both the optical and the electrical properties of the nanostructured silicon solar cells. In fact, the behavior that the surface reflectance decreases with increasing silicon nanostructure density (in a certain range) also suggests that a shorter nanostructure height is required to obtain an excellent optical absorption for higher nanostructure density. Jung et al.[27] have demonstrated that a nanostructure height of only 1.2 μm is required to obtain 99% absorption for a nanostructure density of 38%, while a density of 12% requires a height of 6 μm to obtain the same absorption, as illustrated in Figure 2c. This results in a dramatic reduction of the surface area and an improved blue spectral response; thus, a much higher short-circuit current density (J_{SC}) and open-circuit voltage (V_{OC}) have been obtained for the cell with a nanostructure density of 38% (shown in Figure 2d). Therefore, one of the key factors for the optimal design of nanostructured silicon solar cells is the realization of relatively short and dense silicon nanostructures to obtain a superior light absorption while maintaining a low surface recombination rate.

Besides the multiscale surface texture and optimization of silicon nanostructure density, novel silicon nanostructures with low surface area enhancement have also been proposed and investigated in an attempt to restrain the surface recombination. Gao et al.[29] have reported a low aspect ratio honeycomb nanobowl structure (see Figure 2e), which is formed by firstly oxidizing silicon nanopores and then removing the oxide layer. During the etching process, the initial 450-nm-deep cylinder-like pores with diameters ranging from 30 to 60 nm evolve into 200-nm-deep nanobowls with diameters of about 120 nm at the top and 70 nm at the bottom, indicating a significant decrease in aspect ratio. Therefore, the surface area enhancements of the honeycomb nanobowl structures (only 2 times compared to the planar surface) are much lower than that of their initial nanopore structures (5.8 times compared to the planar surface), which exhibits a great potential for reducing

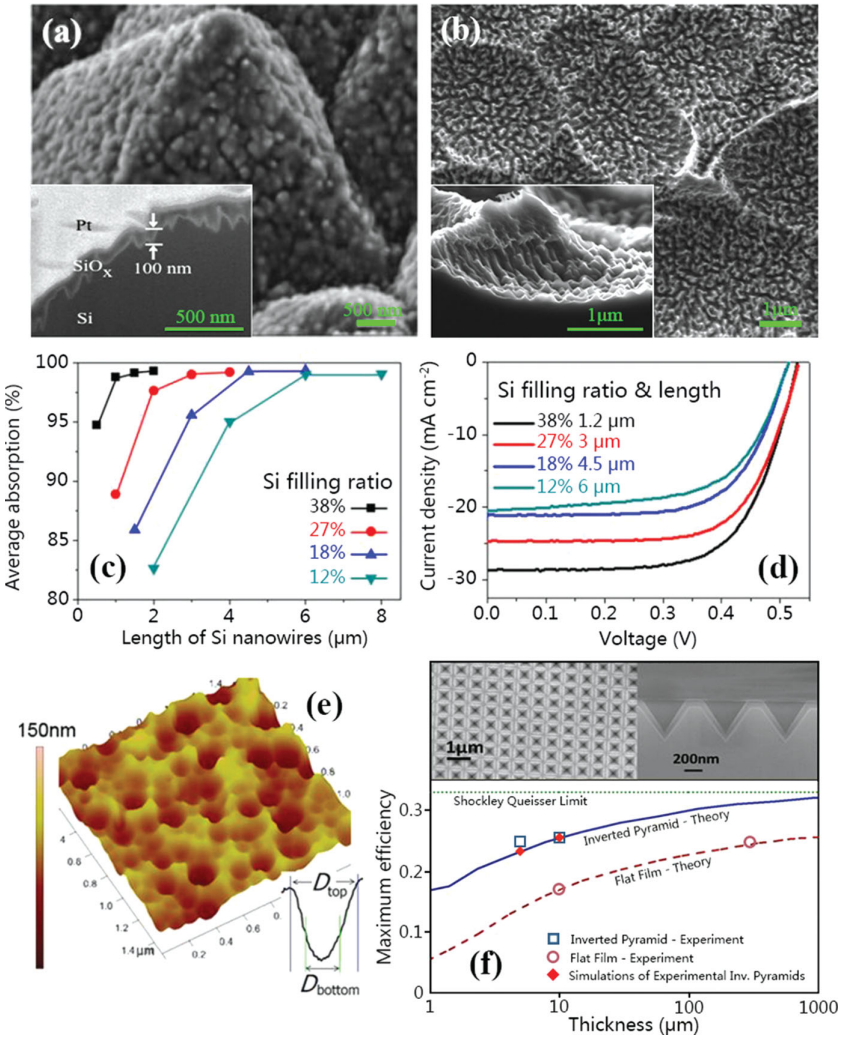

Figure 2. Tilted top-view scanning electron microscope (SEM) images of the multiscale textured surface for: a) the crystalline silicon and b) multicrystalline silicon solar cells. The insets are the cross-sectional SEM images of the corresponding multi-sale structures. c) Average absorption of the silicon nanostructure samples with different filling ratios and nanostructure lengths. d) Typical *I*–*V* characteristics of the nanostructured silicon solar cells depending on the combination of filling ratio and nanostructure length. Note that all these cells have the same light absorption of 99%. e) 3D scanning probe microscopy image of the honeycomb nanobowl structure. f) SEM images of the inverted nanopyramid array with a period of 700 nm (top) and maximum efficiency at normal incidence as a function of silicon wafer thickness for inverted nanopyramids and planar films (bottom). a) Reproduced with permission.[25] Copyright 2011, American Institute of Physics. b) Reproduced with permission.[36] Copyright 2014, Elsevier B. V. c,d) Reproduced with permission.[27] Copyright 2013, Elsevier B. V. e) Reproduced with permission.[29] Copyright 2013, AIP Publishing LLC. f) Reproduced with permission.[28] Copyright 2012, American Chemical Society.

surface recombination. Moreover, a lower surface reflectance is achieved for the honeycomb nanobowl structures due to the more effective impedance matching and photonic light trapping,[29] despite their lower aspect ratio. It has also been observed that nanocone solar cells possess superior external quantum efficiency (EQE) due to their minimal increment of surface area. The surface area increment of the nanocone structure with a height of 400 nm and a diameter of 450 nm is only 67% as compared with the planar surface, a value much lower than that of the nanopore or nanowire structure.[24] Also, considerable interest is focused on the inverted nanopyramid structure due to its surface area enhancement ratio of only 1.7-fold. With an attempt to enhance the performance of the nanostructured silicon solar cells, Mavrokefalos et al.[28] have fabricated a periodic inverted nanopyramid structure by standard scalable microfabrication techniques based on interference lithography and wet Si etching to deeply investigate its optical properties. They have demonstrated that a 5-μm-thick silicon wafer with such inverted nanopyramids can absorb as much light as a 300-μm-thick planar wafer does, resulting in their comparable maximum efficiencies, as shown in Figure 2f. Meanwhile Shi et al.[38] have reported a random inverted nanopyramid structure formed by Ag-catalyzed chemical etching followed by NaOH modification and shown its effectiveness in improving solar-cell performance. Compared with nanoporous solar cells, inverted nanopyramid solar cells exhibit a remarkably improved blue spectral response and diode parameters (ideality factor and reverse saturated current density), indicating the decrease of surface recombination, which leads to a great increase in V_{OC} and J_{SC}.[38]

3. Reducing Emitter Recombination by Controlling Emitter Volume and Doping Concentration

Carrier recombination within the emitter is particularly severe for the nanostructured silicon solar cells due to its sensitivity on the emitter volume and doping concentration. For the purpose of determining the influence of nanostructure height (thus emitter volume) on the carrier recombination, we have performed a thorough investigation of the nanostructured silicon solar cells (with silicon nanowire-like surface morphology) based on the internal quantum efficiency (IQE),[16] as shown in **Figure 3**a. The three samples labeled A3, A5, and A10 correspond to the nanostructure heights of 300, 500, and 1000 nm, respectively. It is found that the IQE decreases over the whole wavelength range with increasing nanostructure height, particularly in the short-wavelength range. On the one hand, this is a result of the enhanced surface recombination caused by the increment of the surface area; on the other, the lateral feature size of the silicon nanostructures is around 50 nm, which is an order of magnitude smaller than the diffused junction depth in a polished wafer. Since the doping concentration approximately decreases in the form

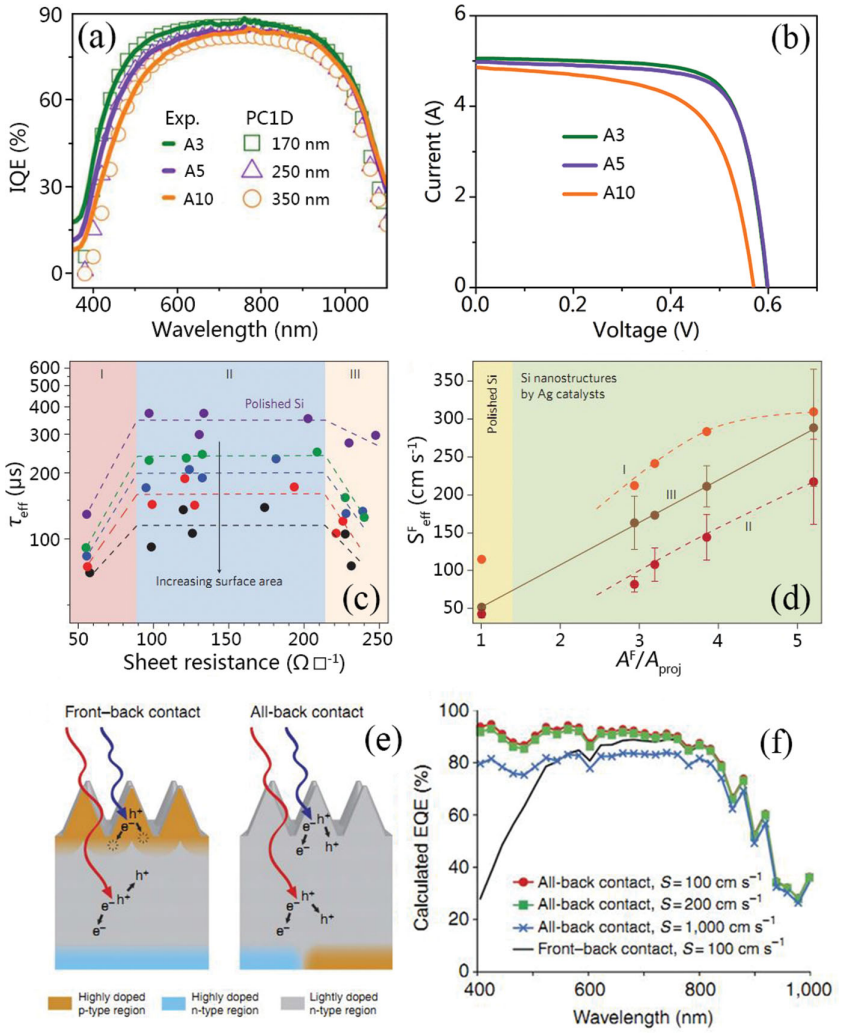

Figure 3. a) Experimental IQE spectra (curves) and the calculated IQE results from PC1D simulations (scatter points) of the cells from different groups with the nanostructure heights of 300, 500 and 1000 nm. The numbers in the PC1D legend indicate the corresponding thicknesses of the "dead layers". b) Current–voltage characteristics of these nanostructured silicon solar cells, which correspond to the electrical parameters in Table 1 of ref. [16] c) τ_{eff} of the nanostructured silicon wafers versus R_s. The dashed lines are a guide to the eye. Regions I, II, and III delineate three different regimes of τ_{eff} determined by R_s. d) S^F_{eff} in different R_s region as a function of A^F/A_{proj}. e) Shematics of front-back-contact and all-back-contact silicon solar cells. f) Calculated EQE of four different nanostructured silicon solar cells with the front-back-contact and all-back-contact design. a,b) Reproduced with permission.[16] Copyright 2013, IOP Publishing, Ltd. c,d) Reproduced with permission.[35] Copyright 2012, Macmillan Publishers Limited.[35] e,f) Reproduced with permission.[24] Copyright 2013, Macmillan Publishers Limited.

of a complementary error function from the surface to the depletion region, it can be readily concluded that the doping concentration within the whole nanostructure approaches the surface peak value, leading to both severe Auger and Shockley–Read–Hall (SRH) recombination within the emitter bulk. These features make the nanostructured emitter behave as a "dead layer".[39] By employing PC1D software, the thicknesses of the "dead layers" are calculated to be 170, 250, and 350 nm for the A3, A5, and A10 silicon nanostructures, respectively. It can thus be concluded that higher nanostructures (larger emitter volume) produce thicker "dead layers" and more-severe carrier recombination, leading to a degraded cell performance (see Figure 3b).[16]

Another significant approach to suppress the emitter recombination is the control of the doping concentration, embodied by the change of the sheet resistance (R_s). Oh et al.[35] have deeply investigated the influence of R_s on carrier recombination and identified the regimes of R_s in which the cell performance is primarily limited by surface recombination or Auger recombination. As shown in Figure 3c, the effective minority carrier lifetimes (τ_{eff}) of all given nanostructured silicon wafers increase as R_s increases from 55 to 100 Ω □$^{-1}$ (Region I) and then stay almost unchanged for R_s between 100 and 200 Ω □$^{-1}$ (Region II). When further increasing R_s (Region III), τ_{eff} decreases due to the weakening of the built-in electric field. It is evident that the carrier recombination is strongly influenced by R_s. To further identify the dominant carrier recombination mechanism of the nanostructured silicon wafer in each doping region, they have deduced an equation to reveal the relationship between S^F_{eff} and A^F/A_{proj}, namely:[35] $S^F_{eff} = S^F_{loc}\frac{A^F}{A_{proj}}$, where S^F_{eff} denotes the effective surface recombination velocity at the front surface, S^F_{loc} is the local effective surface recombination velocity at and very near the actual front surface, and A^F/A_{proj} is the surface area enhancement ratio. Obviously, S^F_{eff} should depend linearly on A^F/A_{proj} if surface recombination dominates among all carrier recombination mechanisms (thus S^F_{loc} is a constant value), which is true in the light doping region (Region III), as shown in Figure 3d. However, in the heavy doping region (Region I), S^F_{eff} severely deviates from the linear dependence on A^F/A_{proj}, indicating the dominance of the Auger recombination; and in the moderate doping region II, S^F_{eff} slightly deviates from the linear dependence on A^F/A_{proj}, suggesting that the contribution from both mechanisms should be considered.

As is now widely acknowledged, the suppression of Auger recombination through controlling the doping concentration is extremely important for the nanostructured silicon solar cell due to the high aspect ratio of its surface morphology. Oh et al.[35] have achieved an 18.2%-efficient nanostructured c-Si solar cell with a size of 0.8 cm^2 by adopting a high sheet resistance of 129 Ω □$^{-1}$ (in Region II) and optimizing the surface morphology. In theory, the use of very light doping (such as in region III) may reduce significantly Auger recombination; however, it is not adopted in nanostructured silicon solar cells with conventional front-back-contact design because of the weakening of the built-in electric field and the dramatic increase of series resistance. Recently,

Jeong et al.[24] demonstrated that all-back-contact design can effectively solve this dilemma and improve the power conversion efficiency of nanostructured silicon solar cells. Compared with the front-back-contact design, the all-back-contact cells have no heavily doped region on the front surface where the nanostructures reside, instead, the emitter layer is designed at the back of the solar cells, as illustrated in Figure 3e. Hence the Auger recombination in the silicon nanostructures is reduced, leading to a pronounced improvement of blue spectral response even if its surface recombination velocity (S) is 10 times that of the front-back-contact ones (see Figure 3f). Due to the increased light absorption and the minimized loss of photogenerated carriers, the J_{SC} of the all-back-contact nanostructured silicon solar cell is 30.7% higher than that of the planar counterpart.

4. Suppression of Carrier Recombination by Dielectric Passivation Coating

Various passivation layers such as thermally grown SiO_2,[35,40] carbon thin films,[33] plasma-enhanced chemical vapor deposited (PECVD) SiN_x layers[32,41] and atomic-layer-deposited (ALD) Al_2O_3 coatings[34] have been widely studied to improve the electrical characteristics of planar or nanostructured silicon solar cells. The passivation effect of the dielectric coatings are generally attributed to two mechanisms: chemical passivation by decreasing the interface defect density (such as by forming Si-O bonds in the case of SiO_2 coating and Si–H bonds in the case of hydrogen-containing PECVD SiN_x coating) and field-effect passivation by repelling the electrons or holes away from the surface (such as by the negative fixed charges in Al_2O_3 and positive fixed charges in SiN_x). Thermally grown SiO_2 is one of the most popular surface-passivation techniques used to reduce surface defect density owing to its excellent chemical passivation, and has been proved quite effective in suppressing the surface recombination of silicon solar cells (by using SiO_2 as front and back passivation layers, an efficiency of 24.7% has been achieved for the c-Si solar cells).[40] A very low local effective surface recombination velocity of 56 cm s^{-1} on silicon nanostructured surfaces has been reported by using thermally grown SiO_2 as passivation coating,[35] which is almost equal to that of a polished Si surface coated by SiO_2, demonstrating its effectiveness on silicon nanostructures. Combining SiO_2 passivation with light doping, the IQE of the nanostructured silicon solar cell reaches as high as 63.8% at 400 nm, despite a surface area enhancement of 5.2. In fact, in the work of Jeong et al.,[24] the superior EQE in the short wavelength range of the nanostructured ultra-thin silicon solar cell also stems, in part, from the contribution of SiO_2 passivation. Likewise, carbon thin film has also been proven to be a good dielectric passivation layer which effectively prolongs the minority carrier lifetime from 10 μs to 21 μs in silicon nanowires, exhibiting a much better chemical passivation effect than the H-passivation by HF solution.[33] Another important passivation material is the PECVD SiN_x, which has the ability to greatly reduce surface recombination with the additional advantage of easy implementation into the present production line.[41–43] Liu et al.[32] have thoroughly investigated the passivation effect of SiN_x layer on silicon nanostructures by varying the PECVD conditions, including the gas-flow ratio of NH_3 and SiH_4, the deposition temperature, and the deposition time. It is found that a relatively high deposition temperature (450 °C) facilitates the diffusion of hydrogen atoms into the silicon substrate and consequently reduces the number of the recombination centers. Under the optimized deposition temperature, together with the optimized gas-flow ratio ($NH_3/SiH_4 = 6$) and deposition time (500 s), they successfully obtained an η of 16.25% for SiN_x-passivated nanostructured mc-Si solar cells. Excitingly, Liu et al.[36] and Yue et al.[44] have separately reported η values over 18% for large-scale nanostructured mc-Si solar cells by using SiN_x films deposited in an industrial inline PECVD reactor as both a passivation layer and an antireflection layer, exhibiting the prospect of the mass production of nanostructured silicon solar cells. Our group has thoroughly studied the passivation effect on large-scale (125 mm × 125 mm) nanostructured silicon solar cells with a nanostructure height of 300 nm and coated with SiN_x (D3), SiO_2 (B3), and SiN_x/SiO_2 dual-layer coatings (C3), respectively.[16] We have found that the effective surface recombination velocities of B3, C3, and D3 solar cells are distinctly lower than that of the unpassivated one (A3), revealing the effective suppression of the SRH recombination by these dielectric passivation layers. Moreover, the C3 group shows the lowest effective surface recombination velocity, implying the best passivation effect of SiN_x/SiO_2 dual-layer coating. We attributed its excellent passivation effect to the combined contribution from both the SiN_x and SiO_2 passivation layers. On the one hand, SiO_2 coating provides effective chemical passivation; on the other, the SiN_x coating can realize both a good hydrogen passivation and a field-effect passivation. As a result, C3-group solar cells achieve the best output performance among the four nanostructured silicon solar cells with an open-circuit voltage of 0.620 V and a short-circuit current of 5.54 A, which is illustrated in **Figure 4**a.

Recently, the conformal ALD-Al_2O_3 coating has attracted lots of interest as a passivation layer for planar and nanostructured silicon surfaces: it not only yields a good chemical passivation, but also results in a strong field effect passivation due to the fixed charges at the interface of Si/Al_2O_3.[45–48] In ALD-Al_2O_3-passivated black silicon, an ultra-low surface recombination velocity of 13 cm s^{-1} has been reported, which is similar to its planar counterpart, proving the excellent passivation effect on silicon nanostructures.[34] Wang et al.[49] compared the passivation effect of the as-deposited and forming-gas-annealing (FGA) (the forming gas is a mixture of nitrogen and hydrogen) treated ALD-Al_2O_3 by high-frequency capacitance–voltage (C–V) measurements. From the C–V curves in Figure 4b, the flatband voltages can be calculated, and thus the interficial defect density (D_{it}) can be aquired. The D_{it} of the FGA-treated Al_2O_3 is 1.37×10^{11} cm^{-2}, almost an order of magnitude lower than that of the as-deposited Al_2O_3 (1.2×10^{12} cm^{-2}), which is ascribed to the passivation of interficial states by molecular hydrogen contained in the forming gas. Due to the enhanced suppression of surface recombination by FGA-treated Al_2O_3, they have successfully realized a nanostructured c-Si solar cell with an η of 18.2%, a significant improvement over those with no passivation (η = 16.5%) or with as-deposited Al_2O_3 passivation (η = 17.7%). Utilizing ALD-Al_2O_3 as a passivation layer, Repo et al.[50] also reported a high-efficiency (18.7%) nanostructured

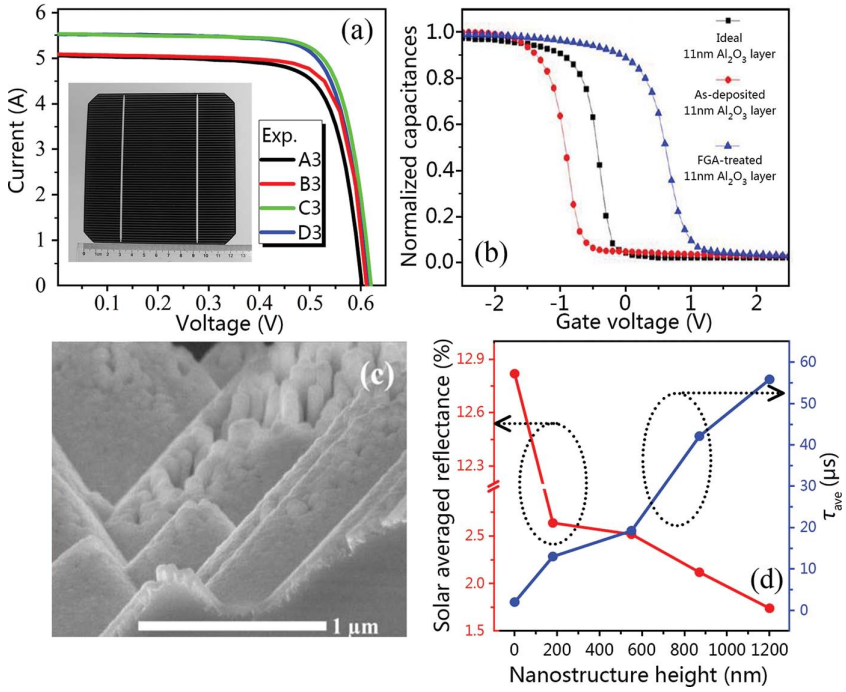

Figure 4. a) Current–voltage curves of the A3, B3, C3, and D3 group nanostructured silicon solar cells under AM 1.5G illumination, together with an image of the C3 group cell shown in the inset. b) Normalized *C–V* curves of the Ni/Al_2O_3/Si capacitors with an 11 nm-thick ideal/as-deposited/FGA-treated Al_2O_3 layer, respectively. c) SEM image of the ALD-Al_2O_3-coated silicon nanostructures on the pyramid texture. d) Dependence of the solar averaged reflectance and averaged effective minority carrier lifetime τ_{ave} on nanostructure height in the ALD-Al_2O_3-coated silicon multiscale surface texture. Note that the data are extracted from Table 1 of ref. [51] (the corresponding nanostructure heights can also be found in that text). a) Reproduced with permission.[16] Copyright 2013, IOP Publishing, Ltd. b) Reproduced with permission.[49] Copyright 2013, American Chemical Society. c,d) Reproduced with permission.[51] Copyright 2014, John Wiley & Sons, Ltd.

c-Si solar cell on an *n*-type wafer (the others reported in this Research News article are all *p*-type) with an area of 4 cm^2, benefiting from the low surface recombination and good antireflection property. We have applied the ALD-Al_2O_3 coating to large-scale (125 mm × 125 mm) silicon nanostructures on the pyramid texture and successfully obtained a highly conformal morphology of ALD-Al_2O_3 coating as shown in Figure 4c.[51] In order to study the field effect passivation of ALD-Al_2O_3 coating, we have also examined the corona charge–voltage properties of ALD-Al_2O_3-passivated planar and nanostructured silicon surfaces, from which the flat band voltages are determined and the fix charge densities are calculated to be as high as -3.65×10^{12} and -3.09×10^{12} cm^{-2}, respectively, directly evidencing the strong field-effect passivation.[51] In general, higher silicon nanostructures result in lower reflection but severer surface recombination. However, we have demonstrated in the ALD-Al_2O_3-passivated silicon nanostructures that the solar averaged reflectance decreases but the averaged effective minority carrier lifetime τ_{ave} increases with increasing silicon nanostructure height, as is illustrated in Figure 4d. This novel property is attributed to the enhanced field effect passivation in the higher-and-thinner silicon nanostructures, which suggests the possibility of achieving the simultaneous optimization of optical and electrical properties without having to make a trade-off. Therefore the ALD-Al_2O_3-passivation opens a new approach to realize high-efficiency nanostructured silicon solar cells.

5. Conclusion and Outlook

We have reviewed the recent progress in suppressing carrier recombination to promote the conversion efficiency of nanostructured silicon solar cells. The extremely severe carrier recombination comes from both the greatly increased surface area and the much enlarged volume of the heavily doped emitter in silicon nanostructures. Extensive studies have shown that optimal surface morphologies (including multiscale surface texture, relatively high nanostructure density and novel nanostructures with low surface area enhancement) and suitable dielectric passivation layers (such as SiN_x, SiO_2, and Al_2O_3) are the key to reducing the surface recombination of silicon nanostructures. Meanwhile, the solution to the emitter bulk recombination lies in reducing the emitter volume by decreasing the nanostructure height, as well as lowering the doping concentration. The all-back-contact structure has also been applied to nanostructured silicon solar cells recently, which is a better solution for minimizing the emitter bulk recombination. It should be noted that some of these techniques often reduce both the surface and emitter bulk recombination simultaneously. The surface morphology can influence the emitter bulk recombination while the nanostructure height also affects the surface recombination.

In general, all these techniques should be adopted in a specific nanostructured silicon solar cell to minimize the carrier recombination, and thus realize high-efficiency. Figure 1b summarizes some of the highest-efficient nanostructured silicon solar cells to date, where the main techniques of recombination suppression in each case are labeled accordingly. It is worth mentioning that some of the nanostructured silicon solar cells (highlighted by asterisks) are fabricated on large scale wafers under the present industrial manufacture process and perform better than the conventional counterparts, showing the prospect of mass production of nanostructured silicon solar cells. To further improve the conversion efficiency of nanostructured silicon solar cells on large scale, efforts should be devoted to the application of ALD-Al_2O_3 passivation coating to reduce the surface recombination while maintaining excellent antireflection, together with adopting the all-back-contact structure to maximally suppress emitter bulk recombination. With these techniques to restrain carrier recombination, silicon nanostructures will be a highly prominent platform for the mass production of high-efficiency silicon solar cells.

Acknowledgements

This work was supported by the National Major Basic Research Project (2012CB934302), and the Natural Science Foundation of China (11174202 and 61234005).

Received: April 6, 2014
Revised: June 17, 2014
Published online: September 10, 2014

[1] T. J. Kempa, R. W. Day, S. K. Kim, H. G. Park, C. M. Lieber, *Energy Environ. Sci.* **2013**, *6*, 719.
[2] M. Y. Shih, S. F. LeBoeuf, M. Pietrzykowski, O. V. Sulima, J. Rand, A. Davuluru, U. Rapol, L. Tsakalakos, J. Balch, P. J. Codella, B. A. Korevaar, J. Fronheiser, *J. Nanophotonics* **2007**, *1*, 013552.
[3] T. H. Pei, S. Thiyagu, Z. Pei, *Appl. Phys. Lett.* **2011**, *99*, 153108.
[4] S. E. Han, G. Chen, *Nano Lett.* **2010**, *10*, 4692.
[5] E. Garnett, P. Yang, *Nano Lett.* **2010**, *10*, 1082.
[6] H. M. Branz, V. E. Yost, S. Ward, K. M. Jones, B. To, P. Stradins, *Appl. Phys. Lett.* **2009**, *94*, 231121.
[7] S. Koynov, M. S. Brandt, M. Stutzmann, *Appl. Phys. Lett.* **2006**, *88*, 203107.
[8] J. S. Yoo, I. O. Parm, U. Gangopadhyay, K. Kim, S. K. Dhungel, D. Mangalaraj, J. Yi, *Sol. Energy Mater. Sol. Cells* **2006**, *90*, 3085.
[9] J. W. Leem, Y. M. Song, J. S. Yu, *Opt. Express* **2011**, *19*, A1155.
[10] C. Yeo, J. B. Kim, Y. M. Song, Y. T. Lee, *Nanoscale Res. Lett.* **2013**, *8*, 159.
[11] H. C. Chang, K. Y. Lai, Y. A. Dai, H. H. Wang, C. A. Lin, J. H. He, *Energy Environ. Sci.* **2011**, *4*, 2863.
[12] P. Pignalosa, H. Lee, L. Qiao, M. Tseng, Y. Yi, *AIP Adv.* **2011**, *1*, 032124.
[13] W. Q. Xie, J. I. Oh, W. Z. Shen, *Nanotechnology* **2011**, *22*, 065704.
[14] Q. Yang, X. A. Zhang, A. Bagal, W. Guo, C. H. Chang, *Nanotechnology* **2013**, *24*, 235202.
[15] K. Peng, Y. Xu, Y. Wu, Y. Yan, S. T. Lee, J. Zhu, *Small* **2005**, *1*, 1062.
[16] X. X. Lin, X. Hua, Z. G. Huang, W. Z. Shen, *Nanotechnology* **2013**, *24*, 235402.
[17] D. Kumar, S. K. Srivastava, P. K. Singh, M. Husain, V. Kumar, *Sol. Energy Mater. Sol. Cells* **2011**, *95*, 215.
[18] H. Li, R. Jia, C. Chen, Z. Xing, W. Ding, Y. Meng, D. Wu, X. Liu, T. Ye, *Appl. Phys. Lett.* **2011**, *98*, 151116.
[19] X. Li, J. Li, T. Chen, B. K. Tay, J. Wang, H. Yu, *Nanoscale Res. Lett.* **2010**, *5*, 1721.
[20] Y. Liu, T. Lai, H. Li, Y. Wang, Z. Mei, H. Liang, Z. Li, F. Zhang, W. Wang, A. Y. Kuznetsov, X. Du, *Small* **2012**, *8*, 1392.
[21] S. Wu, L. Wen, G. Cheng, R. Zheng, X. Wu, *ACS Appl. Mater. Interfaces* **2013**, *5*, 4769.
[22] X. Li, Y. Xiao, J. H. Bang, D. Lausch, S. Meyer, P. T. Miclea, J. Y. Jung, S. L. Schweizer, J. H. Lee, R. B. Wehrspohn, *Adv. Mater.* **2013**, *25*, 3187.
[23] L. He, D. Lai, H. Wang, C. Jiang, *Small* **2012**, *8*, 1664.
[24] S. Jeong, M. D. McGehee, Y. Cui, *Nat. Commun.*, **2013**, *4*, 2950.
[25] F. Toor, H. M. Branz, M. R. Page, K. M. Jones, H. C. Yuan, *Appl. Phys. Lett.* **2011**, *99*, 103501.
[26] I. Lee, U. Paik, J. G. Park, *Sol. Energy* **2013**, *91*, 256.
[27] J. Y. Jung, H. D. Um, S. W. Jee, K. T. Park, J. H. Bang, J. H. Lee, *Sol. Energy Mater. Sol. Cells* **2013**, *112*, 84.
[28] A. Mavrokefalos, S. E. Han, S. Yerci, M. S. Branham, G. Chen, *Nano Lett.* **2012**, *12*, 2792.
[29] P. Gao, H. Wang, Z. Sun, W. Han, J. Li, J. Ye, *Appl. Phys. Lett.* **2013**, *103*, 253105.
[30] S. H. Zhong, B. W. Liu, Y. Xia, J. H. Liu, J. Liu, Z. N. Shen, Z. Xu, C. B. Li, *Sol. Energy Mater. Sol. Cells* **2013**, *108*, 200.
[31] S. Krylyuk, A. V. Davydov, L. Levin, A. Motayed, M. D. Vaudin, *Appl. Phys. Lett.* **2009**, *94*, 063113.
[32] B. W. Liu, S. H. Zhong, J. Liu, Y. Xia, C. Li, *Int. J. Photoenergy* **2012**, 971093, DOI: 10.1155/2012/971093.
[33] X. Wang, K. Q. Peng, X. J. Pan, X. Chen, Y. Yang, L. Li, X. M. Meng, W. J. Zhang, S. T. Lee, *Angew. Chem. Int. Ed.* **2011**, *50*, 9861.
[34] M. Otto, M. Kroll, T. Käsebier, R. Salzer, A. Tünnermann, R. B. Wehrspohn, *Appl. Phys. Lett.* **2012**, *100*, 191603.
[35] J. Oh, H. C. Yuan, H. M. Branz, *Nat. Nanotechnol.* **2012**, *7*, 743.
[36] S. Liu, X. Niu, W. Shan, W. Lu, J. Zheng, Y. Li, H. Duan, W. Quan, W. Han, C. R. Wronski, D. Yang, *Sol. Energy Mater. Sol. Cells* **2014**, *127*, 21.
[37] B.-R. Huang, Y.-K. Yang, W.-L. Yang, *Nanotechnology* **2014**, *25*, 035401.
[38] J. Shi, F. Xu, P. Zhou, J. Yang, Z. Yang, D. Chen, Y. Yin, D. Chen, Z. Ma, *Solid-State Electron.* **2013**, *85*, 23.
[39] H. C. Yuan, V. E. Yost, M. R. Page, P. Stradins, D. L. Meier, H. M. Branz, *Appl. Phys. Lett.* **2009**, *95*, 123501.
[40] J. H. Zhao, A. H. Wang, M. A. Green, *Prog. Photovoltaics: Res. Appl.* **1999**, *7*, 471.
[41] S. Duttagupta, F. Lin, M. Wilson, M. B. Boreland, B. Hoex, A. G. Aberle, *Prog. Photovoltaics: Res. Appl.* **2014**, *22*, 641.
[42] A. G. Aberle, *Prog. Photovoltaics: Res. Appl.* **2000**, *8*, 473.
[43] A. Cuevas, M. J. Kerr, J. Schmidt, *Proc. 3rd World Conference on IEEE*, **2003**, *1*, 913.
[44] Z. Yue, H. Shen, Y. Jiang, W. Chen, Q. Tang, J. Jin, T. Pu, J. Luo, F. Kong, C. Rui, J. Cai, *Appl. Phys. A* **2014**, DOI: 10.1007/s00339–014–8414–3.
[45] F. Werner, B. Veith, V. Tiba, P. Poodt, F. Roozeboom, R. Brendel, J. Schmidt, *Appl. Phys. Lett.* **2010**, *97*, 162103.
[46] N. M. Terlinden, G. Dingemans, M. C. M. Van de Sanden, W. M. M. Kessels, *Appl. Phys. Lett.* **2010**, *96*, 112101.
[47] B. Vermang, H. Goverde, L. Tous, A. Lorenz, P. Choulat, J. Horzel, J. John, J. Poortmans, R. Mertens, *Prog. Photovoltaics: Res. Appl.* **2012**, *20*, 269.
[48] H. Lee, T. Tachibana, N. Ikeno, H. Hashiguchi, K. Arafune, H. Yoshida, S. Satoh, T. Chikyow, A. Ogura, *Appl. Phys. Lett.* **2012**, *100*, 143901.
[49] W. Wang, C. Lin, H. Chen, C. Chang, J. Huang, B. Tjahjono, J. Huang, W. Hsu, M. Chen, *ACS Appl. Mater. Interfaces* **2013**, *5*, 9752.
[50] P. Repo, J. Benick, V. Vähänissi, J. Schön, G. von Gastrow, B. Steinhauser, M. C. Schubert, M. Hermle, H. Savin, *Energy Proc.* **2013**, *38*, 866.
[51] Z. G. Huang, S. H. Zhong, X. Hua, X. X. Lin, X. Y. Kong, N. Dai, W. Z. Shen, *Prog. Photovoltaics: Res. Appl.* **2014**, DOI: 10.1002/pip.2506.